B. Wang · Z. Fang

Impacts of shortwave radiation forcing on ENSO: a study with a coupled tropical ocean-atmosphere model

Abstract We describe a coupled tropical ocean-atmosphere model that represents a new class of models that fill the gap between anomaly coupled models and fully coupled general circulation models. Both the atmosphere and ocean are described by two and half layer primitive equation models, which emphasize the physical processes in the oceanic mixed layer and atmospheric boundary layer. Ocean and atmosphere are coupled through both momentum and heat flux exchanges without explicit flux correction. The coupled model, driven by solar radiation, reproduces a realistic annual cycle and El Nino-Southern Oscillation (ENSO). In the presence of annual mean shortwave radiation forcing, the model exhibits an intrinsic mode of ENSO. The oscillation period depends on the mean forcing that determines the coupled mean state. A perpetual April (October) mean forcing prolongs (shortens) the oscillation period through weakening (enhancing) the mean upwelling and mean vertical temperature gradients. The annual cycle of the solar forcing is shown to have fundamental impacts on the behavior of ENSO cycles through establishing a coupled annual cycle that interacts with the ENSO mode. Due to the annual cycle solar forcing, the single spectral peak of the intrinsic ENSO mode becomes a double peak with a quasi-biennial and a low-frequency (4–5 years) component; the evolution of ENSO becomes phase-locked to the annual cycle; and the amplitude and frequency of ENSO become variable on an interdecadal time scale due to interactions of the mean state and the two ENSO components. The western Pacific monsoon (the annual shortwave radiation forcing in the western Pacific) is primarily responsible for the generation of the two ENSO components. The annual march of the eastern Pacific ITCZ tends to lock ENSO phases to the annual cycle. The model's deficiencies, limitations, and future work are also discussed.

1 Introduction

The numerical model that pioneered simulation and prediction of ENSO is an anomaly coupled ocean-atmosphere model of the tropical Pacific (Cane et al. 1986; Zebiak and Cane 1987). The anomaly coupled models (e.g., Anderson and McCreary 1985; Zebiak and Cane 1987; Kleeman 1993; Chang et al. 1994) and their simplified versions (e.g., Neelin 1991; Wang and Fang 1996) are valuable devices in understanding the essential dynamics of ENSO. The success of the anomaly models relies on specification of climatological mean states and a partial coupling (no heat flux coupling). Therefore, these models are unable to address important questions concerning interactions of the mean climate and ENSO and the relationships between external forcing and internal coupled dynamics.

Another class of coupled models involves comprehensive general circulation models of ocean and atmosphere. The earliest realistic simulation of ENSO with a coupled general circulation model (CGCM) was achieved at the Geophysical Fluid Dynamics Laboratory (GFDL)/Princeton University (Philander et al. 1992; Lau et al. 1992) and the Max-Planck Institute (Latif et al. 1993). Recent analyses of 11 coupled general circulation models (CGCMs) indicates that, without flux correction to the mean climate, many CGCMs experience, to various degrees, difficulties in simulating realistic annual cycles (Mechoso et al. 1995). Models producing a realistic mean state without drift do not necessarily produce a good annual cycle. Models producing a realistic annual cycle might have notorious errors in simulated mean states. In addition, models producing reasonable ENSO variability may have poor mean states or annual cycles. The climate drift (Neelin

B. Wang (✉) · Z. Fang
Department of Meteorology and IPRC
School of Ocean and Earth Science and Technology,
University of Hawaii, 2525 Correa Road, Honolulu,
Hawaii 96822, USA
E-mail: bwang@soest.hawaii.edu

et al. 1992) remains a common problem in many fully coupled models. In order to better simulate and forecast ENSO, the coupling was applied to anomalies only, i.e., the climatological mean and annual cycle of the coupled system were fixed when total fields are coupled (Ji et al. 1996). This anomaly coupling technique essentially amounts to the philosophy of anomaly coupled models. Realistic simulation of both climatology and ENSO remains a challenge.

Although CGCMs are capable of simulating interactions between the mean climate and ENSO, their complex and rich physics make it extremely difficult to unambiguously isolate physical mechanisms or conclusively establish the cause of a phenomenon due to a specific process. This, along with the computational expenses, hinders to some extent, rapid improvement of CGCMs.

Our first goal is to develop a coupled tropical ocean-atmosphere model in the spirit of the CGCM, yet computationally efficient. Such a model would fill the gap between simple anomaly models and comprehensive CGCMs. It is in this sense, that the model is termed as intermediate coupled ocean-atmosphere model (ICOAM). The ICOAM is distinguished from anomaly models in that it adopts total coupling and simulates the total fields. It is, therefore, capable of studying interactions between the long-term mean state, the annual cycle, and the ENSO cycles. The ICOAM also is differentiated from CGCM in the sense that the model contains only essential physics necessary for reproducing realistic climatology and interannual variability in some key fields. Thus, its computational efficiency allows a large number of long-term integration and numerical experiments to be performed. The roles of specific physical processes can be readily identified and understood. The knowledge gained from comprehension of ICOAM may offer insights into the behavior of the ENSO modes simulated in complicated CGCMs and observed in the real world. The ICOAM may be a useful tool for understanding the problems that the CGCMs face and providing sharp focus and insightful guidance for designing expensive CGCM experiments.

Our second goal is to verify the performance of ICOAM against observations and to use ICOAM to investigate a fundamental issue: the impact of the annually varying shortwave radiation on ENSO dynamics through the interaction between the coupled annual cycle and ENSO.

2 The coupled ocean and atmosphere model

2.1 The atmosphere model

The atmospheric component of the coupled model is a tropical atmosphere model originally developed by Wang and Li (1993) and improved by Fu and Wang (1998). The model is a two-and-half layer, primitive equation model on the equatorial β-plane. It was aimed at simulating monthly mean tropical surface winds, sea level pressure (SLP), and rainfall for specified lower boundary condi-

tions. The model combines the dynamics of Gill (1980) and Lindzen and Nigam (1987) with parametrization of convective heating, cloud-longwave radiation forcing, boundary layer moist thermodynamics, and surface heat fluxes and wind stress. It features vigorous interactions between the free troposphere flows driven by convective and radiative heating and the boundary flows driven by SST gradient forcing. For details of the model, the readers are referred to Wang and Li (1993) and Fu and Wang (1998). Only major physical parametrizations are briefly discussed in this subsection.

In the free troposphere, the convective heating is determined by both the large-scale forcing (moisture convergence) and the nonlinear dependence of convective instability on underlying sea surface temperature (SST). The latter is based on the assumption that the mean atmospheric conditional instability averaged over the area of model resolution and on a monthly time scale is a nonlinear function of SST, i.e., the heating coefficient δ:

$$\delta = \begin{cases} 1 & \text{if SST } \geq 25.5\ ^\circ\text{C} \\ \frac{(\text{SST}-25.5)}{2} & \text{if } 25.5\ ^\circ\text{C} \leqslant \text{SST} \leqslant 27.5\ ^\circ\text{C and } P_r \geq 0, \\ 0 & \text{otherwise}, \end{cases} \tag{1}$$

where P_r denotes precipitation. The differential longwave radiation cooling is also an important driving force for summer northeast trades and Indian Ocean southwest monsoons (Fu and Wang 1998). The effects of clouds on longwave radiation are represented by a radiation transfer scheme analogous to that of Arakawa et al. (1969). The scheme is based on an empirical transmission function and considers only three types (high, middle, low) of clouds.

The surface heat flux and vertical temperature advection calculated in the boundary layer are critical for realistic simulation of the equatorial surface winds and associated divergence. The model's boundary layer flows and thermal structure are determined by the lower free tropospheric pressure and SST gradient forcing in the presence of friction. The drag coefficient was assumed to be a function of wind speed: $C_d = 0.5\ V_s^{1/2}10^{-3}$, where V_s is surface wind speed (Wu 1969). Thus, an equivalent surface layer Rayleigh friction coefficient is proportional to $V_s^{3/2}$. This wind speed-dependent drag coefficient suppresses otherwise excessively strong surface winds and yields improved entrainment and evaporation cooling rates when the atmosphere model is coupled with the ocean model.

Over the land surface and uncoupled ocean domain, specific humidity q_0 is parametrized as a function of moisture availability and specified surface temperature T_s, i.e.,

$$q_0 = m_a(0.972T_s - 8.92) \times 10^{-3}, \tag{2}$$

where the moisture availability coefficient m_a depends on types of surface coverage classified by Matthews (1983). Over water surface $m_a = 1$, Eq. (2) recovers the empirical formulas used for the tropical ocean which were derived from the regression analysis of COADS (Comprehensive Ocean-Atmosphere Data Set) monthly mean SST and surface specific humidity (Wang 1988; Li and Wang 1994). Over the land surface, eight categories of surface coverage are considered. Their corresponding moisture availability was given based on observations (e.g., Benjamin and Carlson 1986).

The horizontal grid is 4° longitude by 2° latitude. In order to keep computational stability, the Matsuno scheme (Matsuno 1966) was used with a time increment of 20 min. Radiation boundary conditions (Miller and Thorpe 1981) are used at the north and south boundaries to eliminate short wave reflection. The model's run with the same major parameter values as those used in Wang and Li (1993) except that the rainfall efficiency coefficient $b = 0.75$ and the free troposphere Rayleigh friction coefficient $\varepsilon = 3 \times 10^{-6}\ \text{s}^{-1}$.

2.2 The ocean model

The ocean component of the coupled model consists of a mixed layer with variable depth, a thermocline layer in which temperature was assumed to decrease downward linearly, and a deep isothermal inert layer (Wang et al. 1995). The model combines the upper active ocean dynamics and Ekman dynamics described by Zebiak and

Cane (1987) and the mixed layer physics described by Niiler and Krauss (1977). For details of the model, readers are referred to Wang et al. (1995). Only the mixed layer parametrization is briefly described here.

The thermodynamic energy equation for the mixed layer includes nonlinear advection, entrainment, surface heat flux and the penetrated shortwave flux at the base of the mixed layer. The model has a self-contained parametrization scheme for the entrained water temperature, which considers the influences on entrained water temperature from both the thermocline displacement and the variations of the mixed layer temperature and depth. The entrainment rate at the base of the mixed layer is estimated by a modified Niiler–Kraus (1977) scheme. The major modification is the penetrated buoyancy flux due to solar radiation at the mixed layer base. The original formulation contains progressively large errors when the mixed layer becomes shallow. The new scheme takes a more accurate form and overcomes the problem.

The horizontal grid is 2° longitude by 1° latitude. A time increment of three hours was used. The SST at the northern and southern boundaries is relaxed to a climatological annual cycle. The model is running with the same major parameter values as those used in Wang et al. (1995). Realistic coastal lines are used but without mass exchange between the Pacific and other ocean basins.

2.3 Coupling strategy and procedure

The downward heat flux at the ocean surface plays critical role in simulation of long term-mean SST and associated mean atmospheric circulation. Mathematical description of the SST-circulation-cloud-radiation interaction is one of the most taxing problems in climate modeling. Our numerical experiments indicate that inadequate parametrization of the cloud radiation feedback can cause severe climate drift, in particular, when cloud amounts vary explicitly with SST. To keep the simplicity of the intermediate coupled model, we use observed cloud fractions, rather than model-generated cloud fractions, to compute the downward shortwave radiation flux at the ocean surface. The observed cloud fractions include annual cycle.

The surface latent heat flux is another major contributor to the total surface heat flux. The positive feedback between SST and latent heat flux is found to be another source of model climate drift. Special treatment was taken in computing surface latent, sensible, and longwave radiation fluxes. Following Seager et al. (1995), an atmospheric thermodynamic mixed layer of 600 m deep is employed to estimate air specific humidity and temperature. In this scheme, the steady thermodynamic energy and moisture conservation equations are applied in a vertically integrated manner, so that not only SST but also surface winds determine surface air humidity and temperature. In the coupled mode, this scheme can effectively suppress the error growth associated with an inadequate parametrization of latent and sensible heat fluxes and maintain a stable mean climate. The resultant surface latent heat flux compares favorably to that estimated from COADS by Oberhuber (1988) except that the magnitude in the core region of the equatorial cold tongue shows significant discrepancy (figure not shown).

The model atmosphere and ocean cover the global tropics between 30°S and 30°N. In the present study, only the tropical Pacific Ocean actively interacts with the atmosphere. The SST outside the tropical Pacific is specified by the values of the annual cycle. The land surface temperature is specified by 1000 hPa air temperature (ECMWF analysis). In the coastal regions Shuman (1957) smooth scheme is used to provide continuity.

The atmosphere and ocean models are synchronously coupled via both stress and heat fluxes with information being passed between them once per day. No flux correction is applied. The integration of the coupled system starts from the atmospheric and oceanic steady solutions obtained under shortwave radiation forcing in January. No additional initial kicks are needed. Other initial conditions have been used. The resultant interannual oscillations (without annual cycle forcing) have the same statistical characteristics after a few years of adjustment period.

3 Simulated climatology

The annual cycle simulated by the coupled model was derived from model year 41 to year 140 of a control (CTL) experiment that reproduced both the climatology and climate fluctuations ranging from seasonal to multidecadal time scales.

3.1 The long term mean climate

The equatorial mean state, in particular the zonal SST gradient and zonal winds that determine the strength of mean upwelling and the zonal slope of thermocline, is of central importance for a successful simulation of ENSO. The equatorial SST gradient simulated by the present coupled model matches observation well between the dateline and 120°W (Fig. 1a). Major discrepancies are associated with an eastward shift of the locations of the maximum and minimum SSTs. The model also reproduces excellent equatorial zonal winds across the basin except that near the equatorial South American coast where westerlies are excessively strong (Fig. 1b).

In the tropical Pacific, the long-term mean surface winds are in excellent agreement with observations (Fig. 2a, b). The only significant discrepancy is found near the South and Central America coast where the
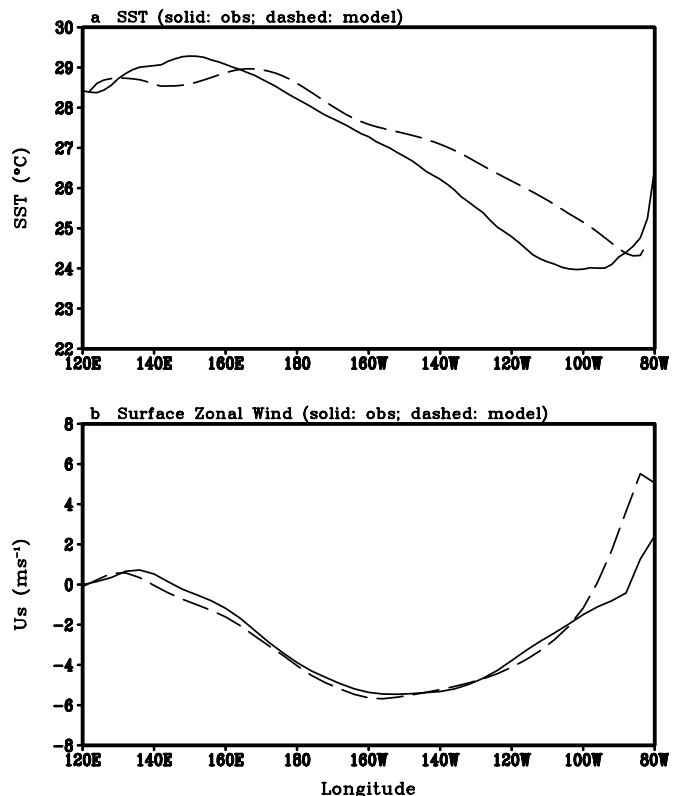

Fig. 1 a Long-term mean SST (°C) and **b** surface zonal winds (ms^{-1}) at the equator. The *solid lines* are derived from COADS (Sadler et al. 1987) and the *dashed lines* are diagnosed from the coupled model

simulated surface winds exhibit excessive westerlies due primarily to lack of topographic blocking effects of the Andes in the model. The excessive westerlies are responsible for the erroneous eastward mixed layer currents in the equatorial far eastern Pacific (Fig. 3a). The simulated rainfall distribution depicts reasonably realistic mean positions of ITCZ and South Pacific Convergence Zone (SPCZ) (Fig. 2a).

The time mean SST field (Fig. 3a) captures gross features of the observed counterpart. Errors exceeding one degree are mainly found in the limited areas of the

equatorial eastern Pacific, southeastern Pacific, and SPCZ (Fig. 3b). These deficiencies are related to an overall eastward shift of the warm water pool. The large errors off coast of Peru are attributed to underestimated coastal upwelling and lateral mixing. The excessive onshore zonal wind produces positive SST errors in the eastern equatorial Pacific. The simulated mixed layer currents (Fig. 3a) are stronger than observed in the equatorial western Pacific. The western boundary currents are weak due to insufficient resolution near the boundary and due to insufficient wind stress forcing

Fig. 2 a Long-term mean values of the surface wind vectors (the scale is given by the *arrow* in the *upper right corner*) and precipitation rate (mm day^{-1}) simulated by the coupled model. **b** The errors of the simulated minus observed surface winds derived from COADS (Sadler et al. 1987)
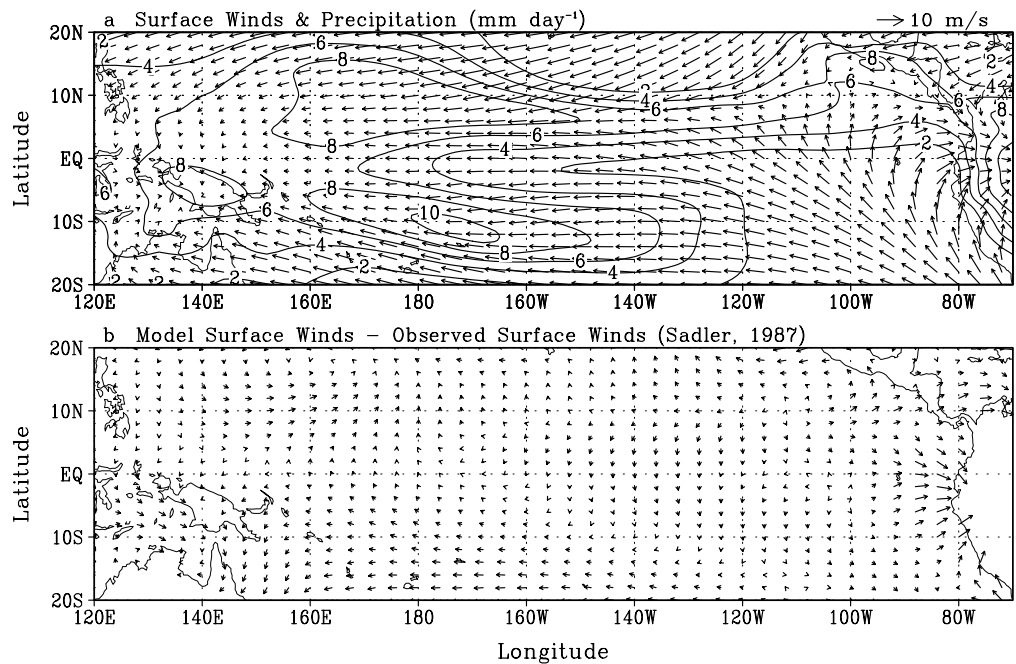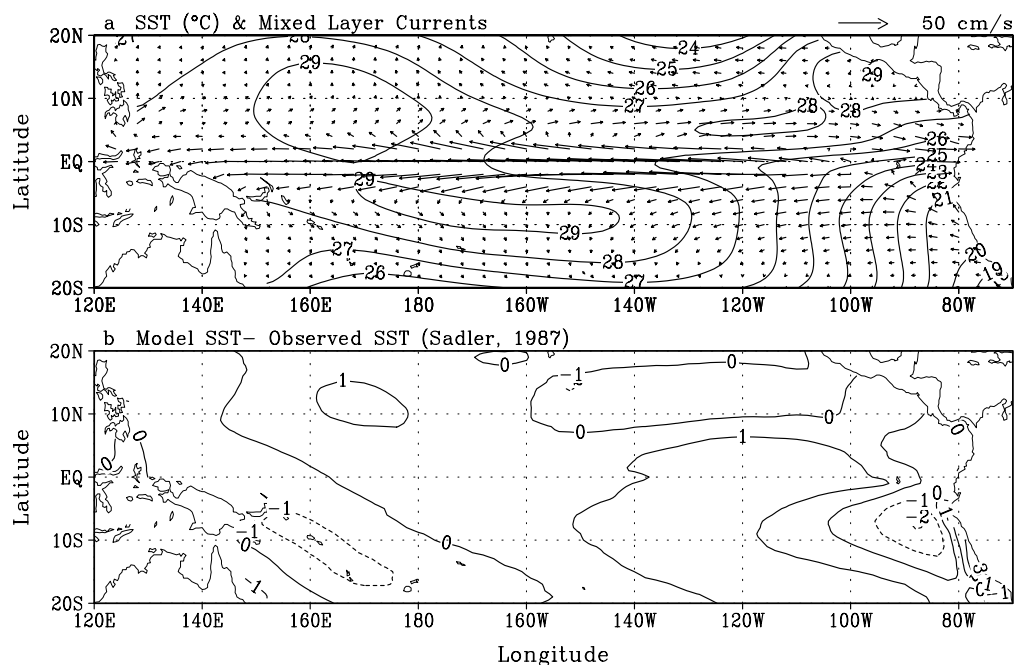

Fig. 3 a The same as in Fig. 2a except for SST (°C) and mixed layer currents (the scale given by the *arrow* in the *upper right corner*). **b** The errors of the simulated minus observed SST derived from COADS (Sadler et al. 1987)

driving the subtropical gyre. In consistence with the positive SST bias east of the Philippine Sea, the mean rainfall there also increases unrealistically compared to observations (Fig. 2a).

3.2 The annual cycle

The annual cycle of the equatorial SST is determined by both the air-sea interaction processes and the influences of the insulation forcing (Wang 1994). Examination of the annual cycle in the equatorial SST provides a critical test for coupled models' physics.

In the eastern Pacific an annual harmonic dominates the simulated annual variation of the equatorial SST (Fig. 4b). Both the amplitude and phase are reasonably realistic comparing with observation (Fig. 4a). The warm phase of the cycle is better captured than the cold phase. The simulated cold phase tends to lag the observed by about one month. The observed westward propagation of warm departure is well reproduced, but the westward propagation of cold departure is exaggerated.

The east-west contrast is one of the essential features of the Pacific climate. To see how the coupled model reproduces this feature, we compare the annual cycles of SST (Fig. 5) and precipitation rates (Fig. 6) averaged over the western (140°E–180°E) and the eastern (120°W–80°W) Pacific.

In the western Pacific, the observed SST maximum (the thermal equator) crosses the equator in June and December following the solar radiation forcing with a time lag about two-three months (Fig. 5a). The coupled model fairly realistically simulates this. In sharp contrast, in the eastern Pacific, the maximum SST is always located in the Northern Hemisphere (Fig. 5b). The thermal equator is closest to the equator (about 6°N) during the warm season in March, whereas it reaches the northernmost position (around 15°N) during the cold season in September. The simulated cycle resembles closely the observed with a moderate phase delay.

The maximum rainfall indicates the location of ITCZ. In the western Pacific (Fig. 6a), the observed rainfall maximum is located around 7°S during boreal winter from December to March while between 3°N and 9°N from April to November. The northernmost location occurs in September. In terms of amplitude and latitudinal locations, the simulated summer monsoon rains in both hemispheres are quite realistic. An abrupt shift of ITCZ from the Southern to the Northern Hemisphere occurs in April and a reversed jump in December. However, the simulated sudden shift of the ITCZ from the Southern to Northern Hemisphere occurs in May. The reason is not clear. In the eastern Pacific (Fig. 6b), the observed ITCZ is located to the north of the equator all year around. In March (September), its position is closest (most remote) to the equator. The heaviest rainfall occurs in July. Double
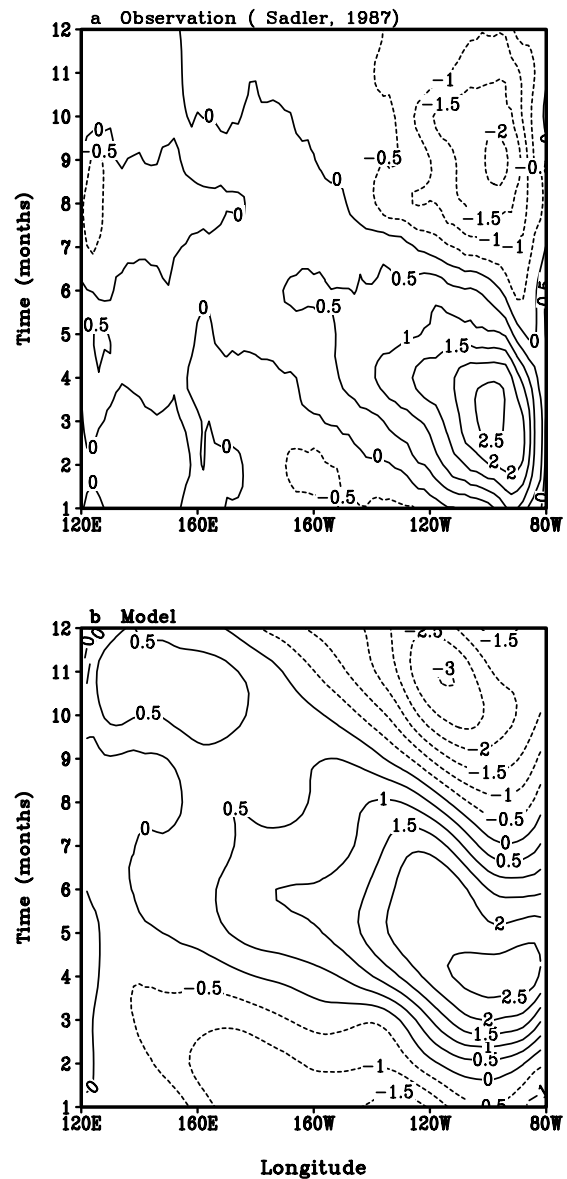

Fig. 4a, b Climatological annual cycle of the equatorial SST deviations (°C) from the long-term means (shown in Fig. 1) derived from **a** the coupled model control run and **b** COADS (Sadler et al. 1987)

ITCZs occur briefly around March. The simulated ITCZ captures these observed features, although the phase of the annual march tends to be delayed by about one month in accord with the delay in the SST annual cycle.

In summary, the coupled model reproduces both the ITCZ in the eastern Pacific and the monsoons in the western Pacific reasonably realistic. Both the annual mean and annual cycle of SST along the equator are better than most of the CGCMs results presented in the intercomparison studies by Mechoso et al. (1995, Figs. 1, 2). An important reason is that in our coupled model we used observed cloudiness to control the downward shortwave flux which apparently plays an
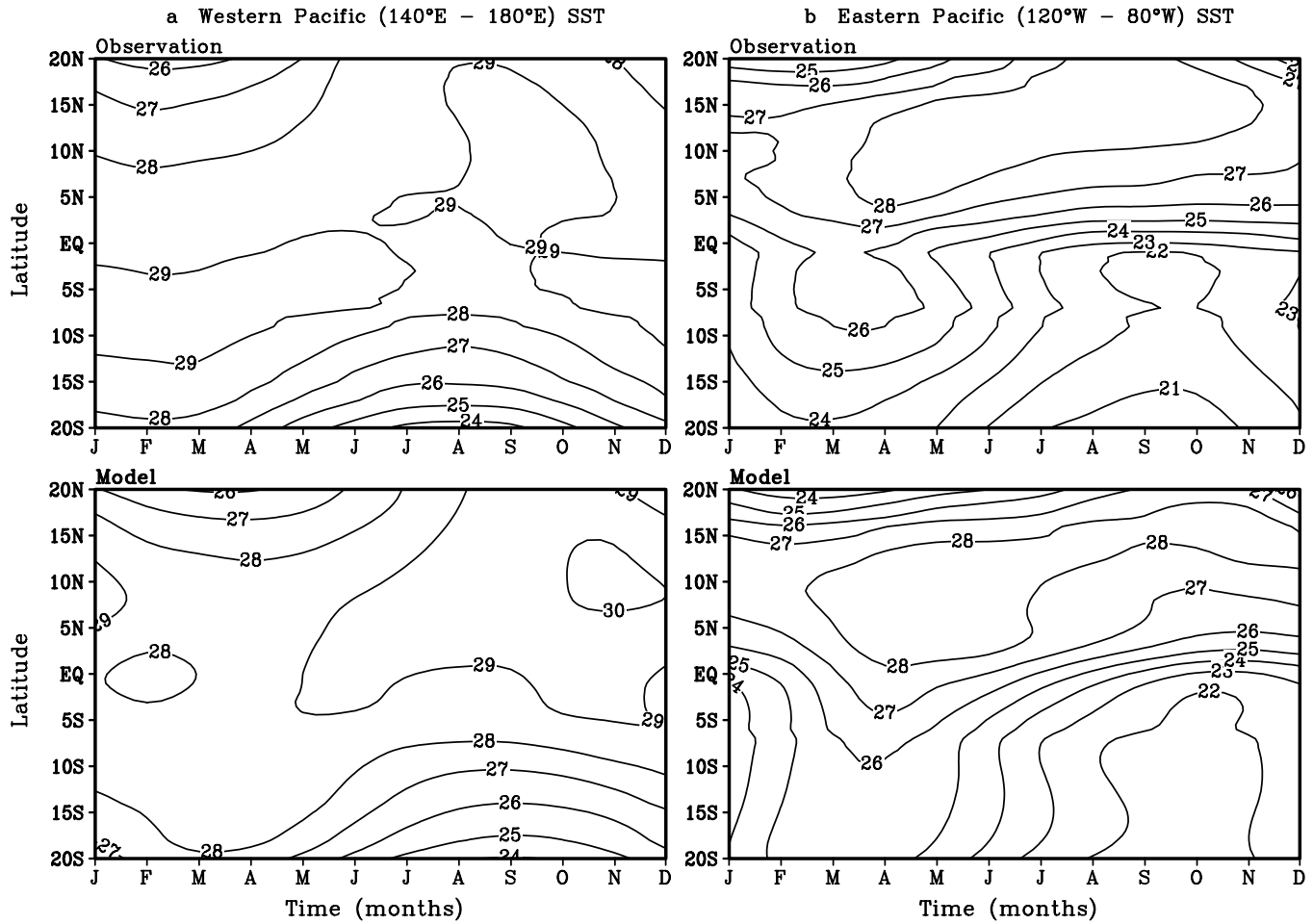
Fig. 5a, b The simulated and observed annual cycle of SST (°C) as a function of latitude averaged over **a** the western Pacific (120°E–180°E) and **b** the eastern Pacific (120°W–80°W)

important role in preventing climate drift and thus producing a realistic climatological mean state. The simulated annual cycle of SST along the equator and averaged over the western and eastern Pacific are sufficiently good for examining its role in generating interannual variation of the coupled model.

4 Simulated interannual variations

4.1 The model ENSO

The model's climate variability in the CTL experiment is highlighted in Fig. 7 in terms of key variables of the ocean and atmosphere (SST, thermocline depth, surface zonal winds, and rainfall) in their corresponding centers of maximum variability. On the interannual time scale, the periods of high SST in the Nino-3 region (5°S–5°N, 150°W–90°W) roughly coincide with the local deep thermocline (Fig. 7a, b). This reflects the essential role of the thermocline displacement in the equatorial eastern Pacific SST variation. To the west of the SST anomalies, the surface westerly and precipitation anomalies in the equatorial central Pacific (150°E–160°W) are nearly in

phase with the Nino-3 positive SST anomalies (Fig. 7c, d). These spatial phase relationships are well observed and can be explained in terms of atmospheric response to underlying SST forcing.

To focus on the ENSO time scale, a seven-month running mean was applied to the time series of the key variables. Figure 8 displays longitude-time diagrams of SST and zonal wind velocity anomalies along the equator. The SST anomalies have two centers; one is located in the far eastern Pacific and the other near the dateline where the mean maximum SST is located (Fig. 8a). These double SST maxima resemble the observed feature showed by Tomita and Yanai (Submitted 1998). In the eastern Pacific, SST anomalies tend to be stationary, while in the western-central Pacific westward propagation is evident. The SST variation is thus characterized by mixed components of standing and westward propagation. The surface zonal winds variation is concentrated in the western Pacific around 160°E, which is in phase with SST variations near the dateline and about 20° longitudes to the west (Fig. 8b). The wind anomalies also show westward propagation, which is coupled with that of the SST anomalies in the western Pacific.
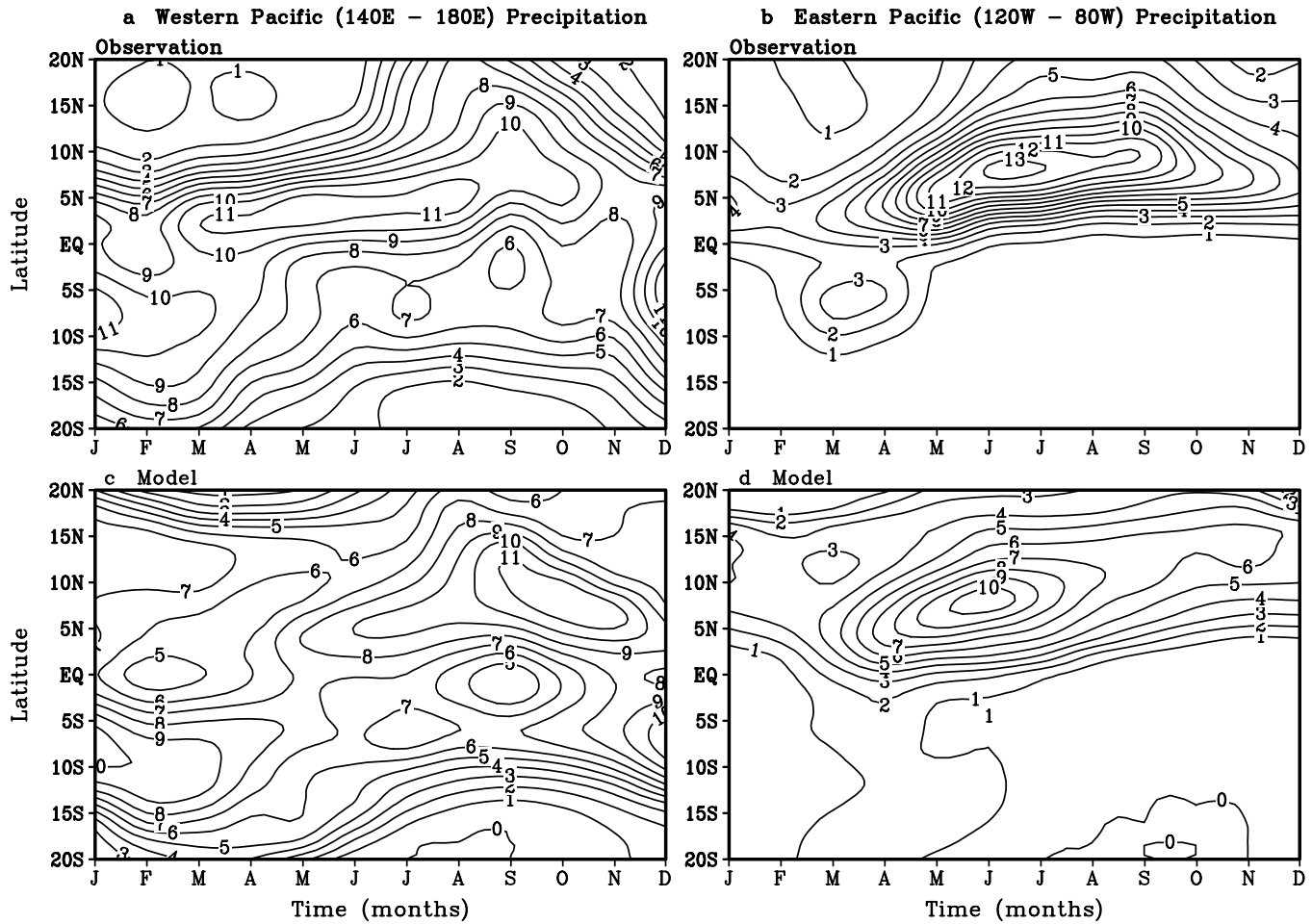
Fig. 6a, b The same as in Fig. 5 except for precipitation rate (mm day^{-1}). The observed rainfall is based on the estimation of Xie and Arkin (1997)

The coupled westward propagation from the central Pacific (160°W) to the western Pacific (140°E) is one of the characteristics of the coupled mode in this model. Since the thermocline is deep in the western-central Pacific, the westward propagation is not due to the air-sea coupling through equatorial upwelling. The remaining candidates are the coupling via surface heat fluxes (latent heat flux) or wind-driven horizontal advection processes. Previous coupled instability analyses suggested that the westward propagating unstable SST mode might originate from the coupled instability, which is associated with zonal temperature advection by currents (Hirst 1986; Neelin 1990). Our diagnostic study shows that zonal temperature advection is indeed a major contributor to the SST variation near and west of the dateline. Figure 9 presents the lag correlation of the zonal advection of temperature along the equator with reference to the SST anomalies at 170°E, which is diagnosed from the model control run. The zonal advection of temperature by currents propagates westward from the dateline to western boundary. Other processes do not show westward propagation.

4.2 Physical mechanisms at work during the model ENSO

The thermocline variations memorize effects of SST on surface winds and provide a delayed feedback to the eastern Pacific SST variations. This is the key process responsible for the cyclic nature of ENSO. To examine thermocline variations associated with ENSO in the CTL experiment, we display thermocline depth anomalies as a function of time along the equator and 5°N (Fig. 10). In the oceanic equatorial waveguide, the simulated thermocline depth anomalies are quasi-stationary in both the western and eastern basins whereas they propagate eastward in the central basin from the dateline to 140°W (Fig. 10a). This feature agrees well with the result of thermocline adjustment within a zonally bounded basin as shown previously by Cane and Moore (1980) and Wakata and Sarachik (1991). The formation of the quasi-standing oscillation in thermocline anomalies involves effects of a family of equatorial Kelvin and Rossby waves and their reflections at the meridional boundaries, especially at the western ocean boundary.

Fig. 7a–d Time series of the following variables simulated in the control experiment: **a** anomalous SST and **b** thermocline depth averaged over the Nino 3 region (5°S–5°N, 150°W–90°W), and **c** anomalous zonal wind and **d** rainfall averaged over the equatorial zone (5°S to 5°N) of the central Pacific (150°E–160°W)
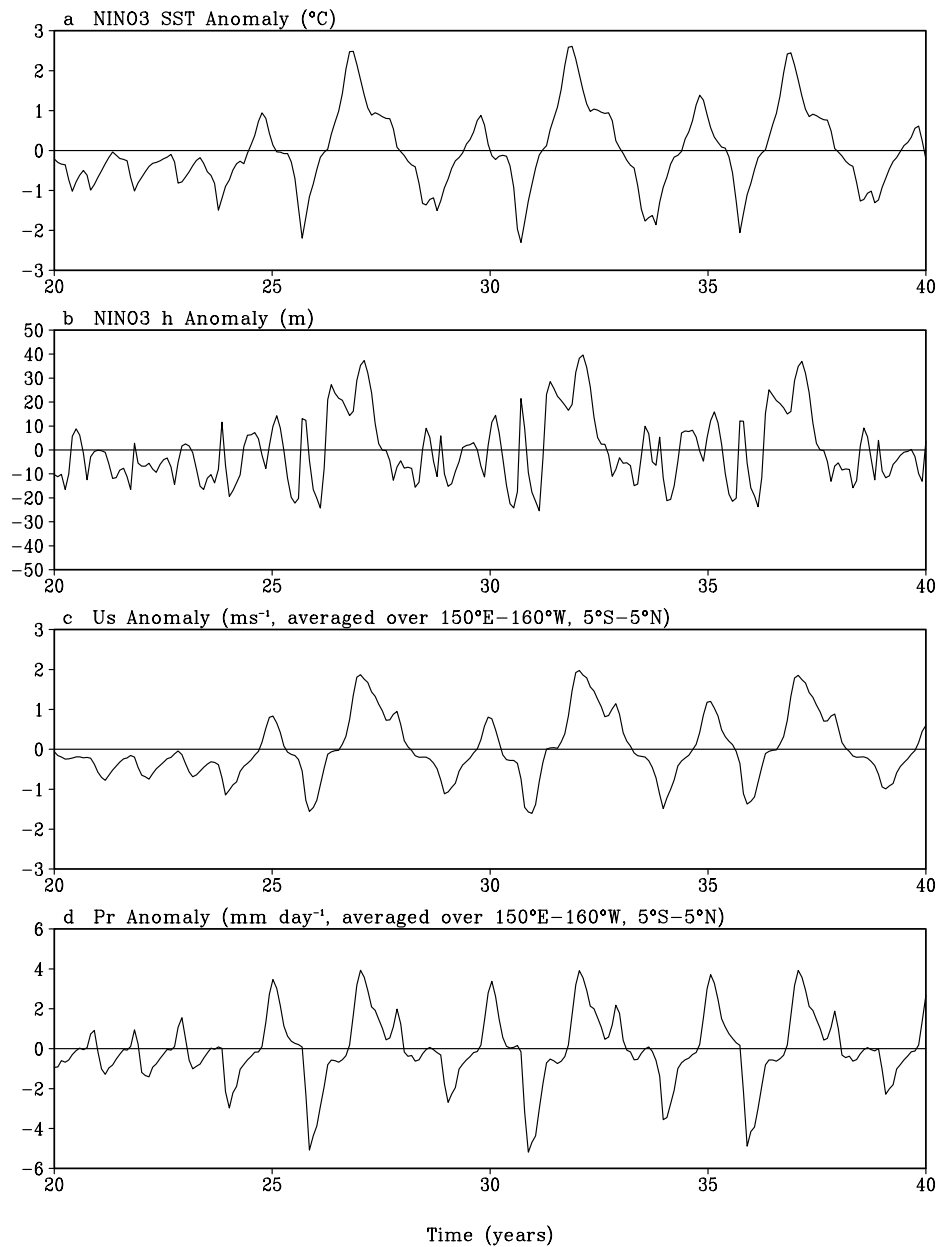

In the off-equatorial latitudes (say 5°N), westward propagation of thermocline depth anomalies dominates (Fig. 10b) which is a sign of the westward propagating equatorial trapped Rossby waves. Figure 10c shows the wind vorticity at 5°N that forces the off equatorial Rossby waves. During each peak warm (cool) phase, the positive wind stress curl anomalies associated with the westerly (easterly) anomalies in the central Pacific excite upwelling (downwelling) Rossby waves on each side of the equator. Comparison of Fig. 10a and b suggests that at the western boundary the upwelling (downwelling) Rossby waves appear to be reflected, contributing to the rise of the thermocline through generating equatorial upwelling (downwelling) Kelvin waves. The Kelvin waves together with the Rossby waves result in an equatorial eastward propagation of

rising (deepening) thermocline into the eastern Pacific. This leads to reversal of warming (cooling) to an opposite trend. On the other hand, Rossby waves reflected at the eastern boundary are evident only for the strong warm events and these waves do not travel across the entire basin, a feature resembling observations (e.g., Wang et al. 1998).

The model oscillation requires two essential elements: local coupled instability and the thermocline adjustment due to equatorial waves. We have performed two experiments to identify the critical processes that maintain the oscillation. In the first experiment, a strong Rayleigh damping (damping time scale of six months) is artificially imposed to thermocline perturbations. This large damping suppresses coupled instabilities and put the coupled system in a stable regime. Although

Fig. 8 a Equatorial SST (°C)
and **b** surface zonal wind (ms^{-1})
anomalies simulated in the
control experiment. *Shading*
indicates *positive SST* and
westerly wind anomalies. The
data were subject to a 7-month
running mean in order to isolate
interannual variation
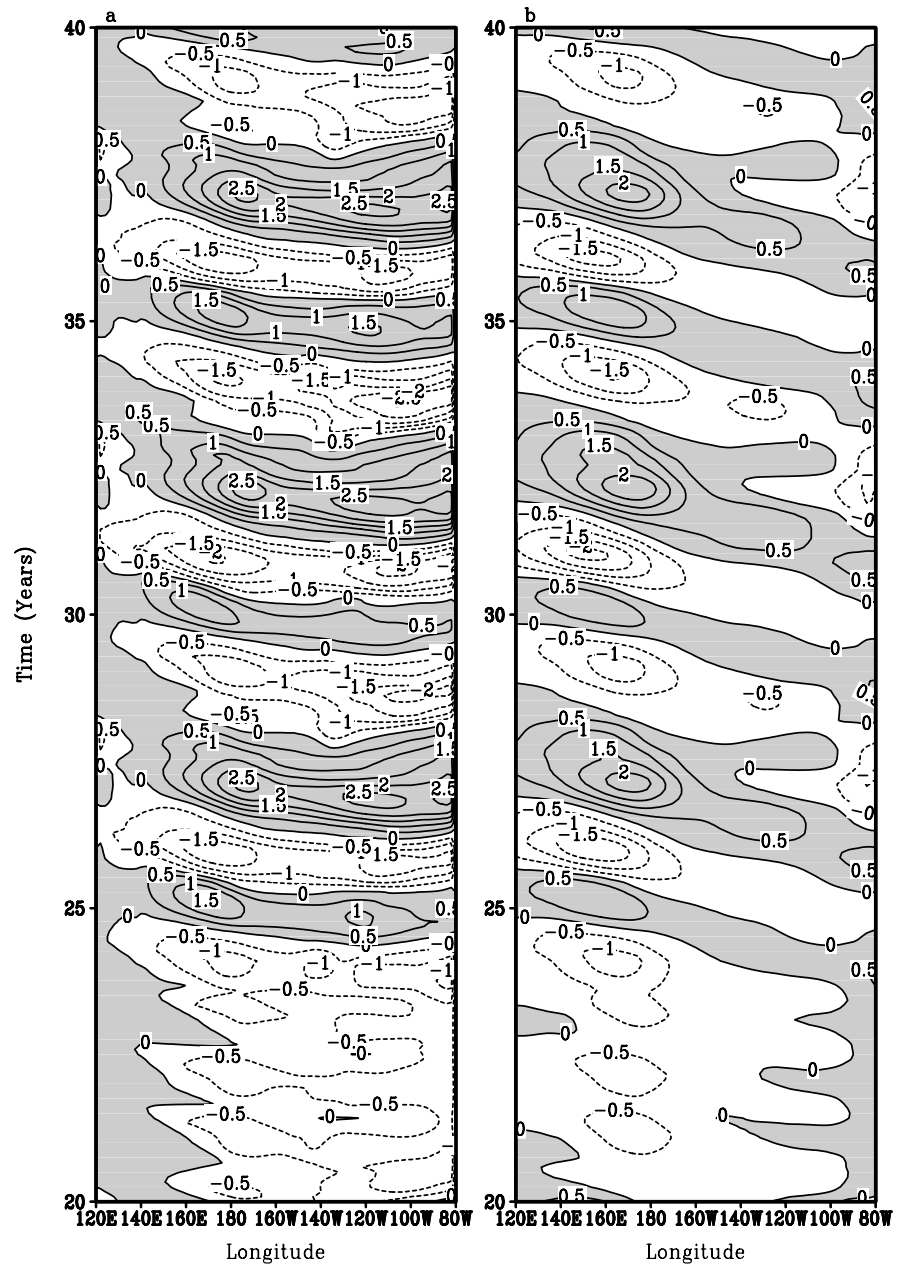
equatorial waves exist, the model exhibits no sustainable oscillation. The initial perturbations were always damped after a few cycles. In the second experiment, we applied a forth order Shapiro filter (Shapiro 1970) at every time step of the ocean model integration, which suppresses large-scale oceanic equatorial waves but has little effect on the coupled instability (slow SST mode). Although the other parameters are identical to the control run, there is no oscillation due to lack of wave activity. These experiments indicate that the coupled instability and the thermocline adjustment due to oceanic waves are two necessary elements for the interannual oscillation of the coupled system. The former amplifies SST perturbations in the eastern Pacific, while the latter provides a negative feedback to shut down the unstable growth and to turn SST toward an opposite

state in the eastern Pacific. These dynamic processes agree with the basic ideas of the delayed oscillator theory (Schopf and Suarez 1988; Suarez and Schopf 1988; Battisti and Hirst 1989) and the standing oscillator model (Wang and Fang 1996).

5 Impacts of the long-term forcing on model ENSO

To identify the effects of the interaction between the annual cycle and ENSO, in this section we study the model ENSO in the absence of the annual cycle by fixing external solar radiation forcing and cloudiness at their annual mean values. For convenience, we refer to this experiment as annual mean forcing (AMF) run. The parameters used in the AMF and CTL experiments are
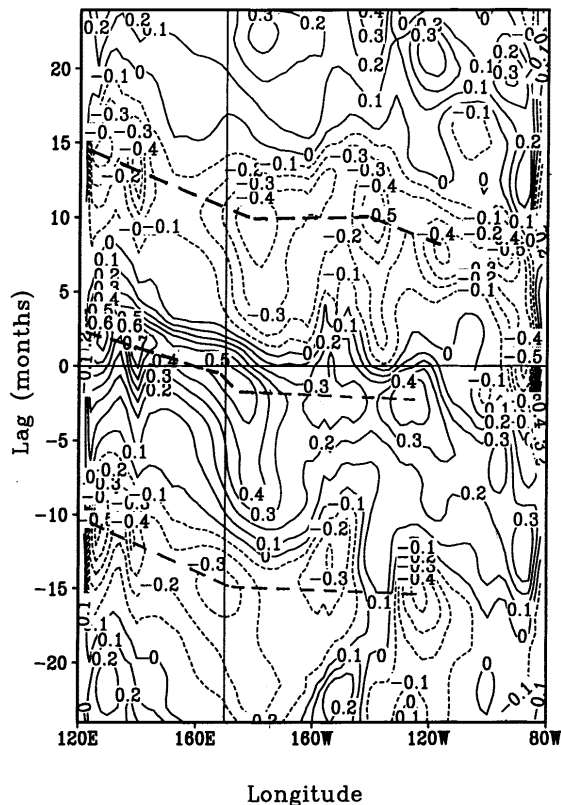
Fig. 9 Time lag correlation between SST anomalies at 170°E and (a) zonal advection of temperature by currents

identical except the external annual cycle forcing in solar radiation and cloud amount.

The long-term mean states derived from the two experiments are very similar (figure not shown). Appreciable differences are found only in the equatorial western Pacific zonal winds. The zonal winds in the CTL run are slightly stronger than those in the AMF experiment, suggesting that the annual cycle of monsoons in the western Pacific has rectified mean zonal winds in the equatorial western Pacific.

The response of the coupled system in the AMF run is dominated by a fairly regular interannual oscillation with a period of about 2.8 years (Fig. 11). The spatial structure and evolution of SST, surface winds, and thermocline depth anomalies resemble the corresponding counterparts in the CTL experiment. This interannual oscillation is an intrinsic mode of the nonlinear coupled system. The oscillation period is determined by the mean state solar radiation forcing for a fixed set of parameters describing atmosphere-ocean coupling.

To see how the oscillation period varies with the mean solar forcing, we designed two additional experiments in which all model parameters are kept identical except that the solar radiation forcing and cloudiness were taken the values of October mean (OctMF) and April mean (AprMF). Figure 12a compares the spectra of the Nino-3 SST anomalies simulated in the three experiments in which annual cycle forcing does not exists.

The oscillation period reduces (increases) from 2.8 years to 2.5 years in OctMF (3.8 years in AprMF). The spatial structure and evolution of the anomalies, however, are similar in all three experiments (figure not shown).

Why does the oscillation period change with shortwave radiation forcing? This is because the shortwave radiation forcing affects ENSO frequency through changing the mean state upon which the ENSO evolves. Figure 12b shows the long-term mean equatorial SST profiles. With October (April) mean forcing, the equatorial SST gradients in the eastern-central Pacific were enhanced (weakened), and so are the corresponding equatorial trades and associated ocean upwelling. The zonal SST gradients and the strength of the equatorial zonal winds and upwelling are stronger under the October forcing; the thermocline slope and associated vertical temperature gradients in the eastern Pacific are also enhanced in the OctMF experiment. The results here imply that enhanced mean upwelling and mean vertical temperature gradients shorten the oscillation period. The question is why. Using a nonlinear dynamic system model, Wang and Fang (1996) showed that the strength of the mean upwelling and the vertical temperature gradients in the equatorial eastern Pacific are two critical parameters that determine the oscillation period for giving coupling coefficients. This is because in the equatorial eastern Pacific, the vertical advection of temperature is the most important process for SST variation. The vertical advection of the mean temperature by anomalous upwelling provides a positive feedback to support unstable growth of SST perturbations as visualized by Bjerkness (1969) and demonstrated by the coupled instability theory (Philander et al. 1984; Hirst 1986). The mean upwelling plays a dual role in ENSO evolution. On the one hand, it favors initial warming. This is because the thermocline deepening leads surface warming, thus during the initial warming the anomalous subsurface temperature exceeds the SST anomalies, i.e., the anomalous vertical temperature gradient is negative. The mean upwelling acting on the negative anomalous vertical temperature favors warming. On the other hand, when the warming reaches a sufficient strength (such that the anomalous vertical temperature gradient becomes positive), the mean upwelling acts to suppress warming and provides a negative feedback. Based on the foregoing analysis, one may infer that when the mean vertical temperature gradients and mean upwelling are stronger, the development of a warm episode and the turnabout from warming to cooling would both be faster, resulting in a shorter oscillation period.

6 Impacts of the annual cycle on ENSO evolution

6.1 Effects of the annual cycle of shortwave radiation forcing

A comparison between the behavior of the coupled system in the control and AMF experiments reveals the
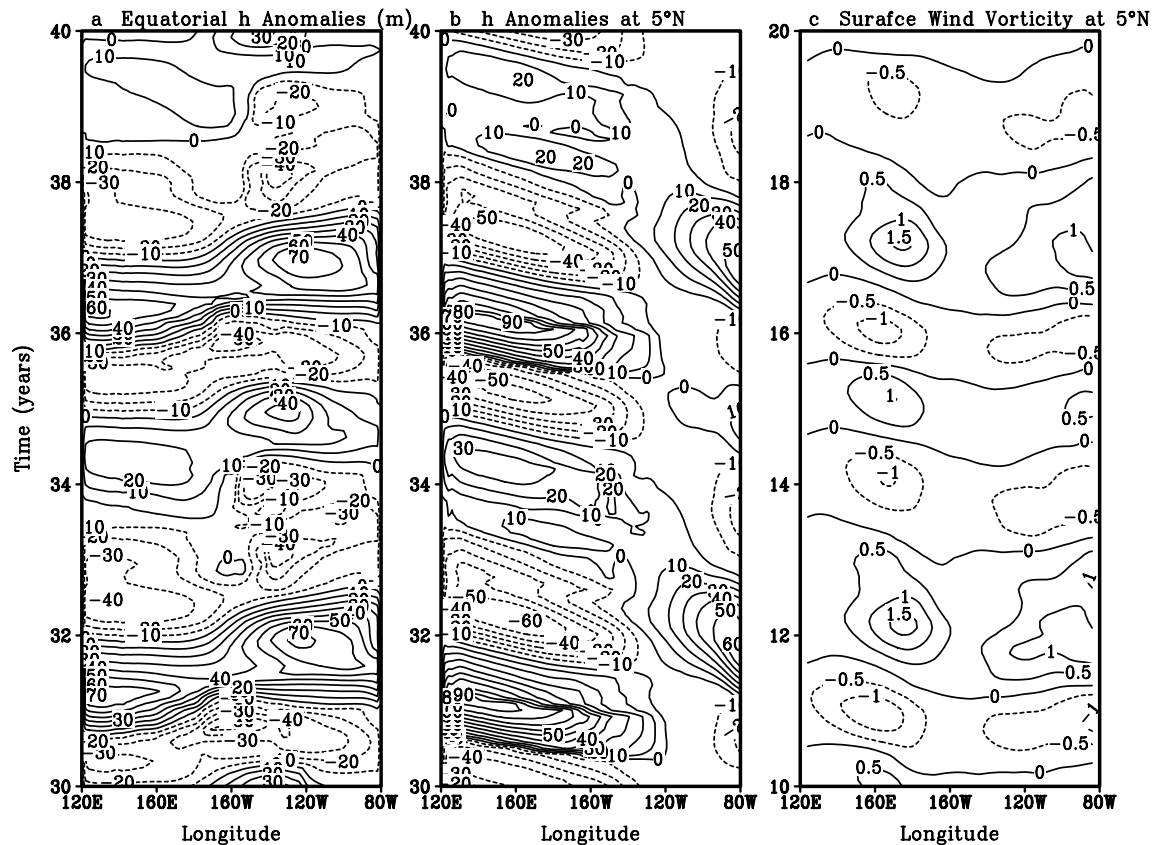
Fig. 10a–c Variations in thermocline depth anomalies (m) **a** along the equator and **b** 5°N simulated in the control experiment from year 30 to 40. **c** The model anomalous zonal winds vorticity $(10^{-6} \, s^{-1})$ at 5°N are presented. All data were subject to a 7-month running mean

effects on the model ENSO of the external annual cycle forcing and the interaction between the annual and interannual variation.

First, the annual cycle forcing significantly changes the periodicity and regularity of the model intrinsic ENSO. As shown by Fig. 11a, with the annual cycle forcing, the spectrum peak is broadened and the intrinsic oscillation with the period of 2.8 years splits into double peaks with a quasi-biennial and a low-frequency (4–5 years) time scale. These two oscillation periods resemble the quasi-biennial and low-frequency components of the observed ENSO (e.g., Rasmusson et al. 1991; Barnett et al. 1991; Rope-lewski et al. 1992). With the annual cycle forcing, the ENSO cycles become irregular due to low-order chaos.

Another fundamental effect of the annual cycle forcing lies in the tendency of locking the phases of ENSO to the annual cycle. Without the annual cycle forcing, the peak warming and cooling of ENSO cycles occur randomly during the course of the year (Fig. 13a). When the annual cycle solar forcing is included, the evolution of ENSO becomes phase-locked to the annual cycle (Fig. 13b). The peak warming occurs preferably in November and peak cooling in September. Both phases prefer the cold season of the equatorial cold tongue. The transition phases tend to concentrate in April and May as seen from the reduced mean positive and negative anomalies (Fig. 13b). This result agrees qualitatively

well with observed behavior of the Nino-3 SST and Southern Oscillation indices (Chang et al. 1996).

Another notable effect of the annual cycle forcing is the conspicuous interdecadal modulation of the amplitude and frequency of the model ENSO. This can be better detected by wavelet analysis of the Nino-3 SST anomaly. The procedure of wavelet analysis was documented in Wang and Wang (1996). The modules of the Nino 3 SST anomaly as a function of time and oscillation period are presented in Fig. 14. The amplitude of the model ENSO varies with time. There are periods during which amplitude is large, for instance from year 10 to 20, year 26 to 42, and year 85 to 95; there are also periods during which the model ENSO is powerless, e.g., from year 45 to 88 and from year 100 to 135. The dominant oscillation period changes with time as well. Biennial oscillation is found from year 45 to 68 and year 95 to 105. The bi-frequency oscillations are evident for the period during year 10–40, year 65–95, and year 115–135 with periods peaking at about 2–3 and 5–6 years. The inter-decadal modulation of the model ENSO frequency and amplitude resembles the observed ENSO behavior (Gu and Philander 1995; Wang and Wang 1996).

In summary, the annual cycle forcing makes ENSO phase-locking to the annual cycle, creates multi-time scales and chaotic behavior, and makes ENSO amplitude and frequency change on an interdecadal time scale.
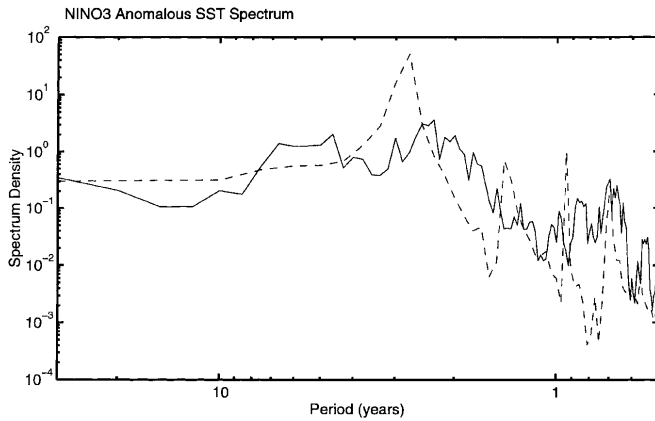
Fig. 11 The spectrum of the SST anomalies simulated in the control experiment (*solid*) and in the annual mean shortwave radiation forcing experiment (*dashed*)
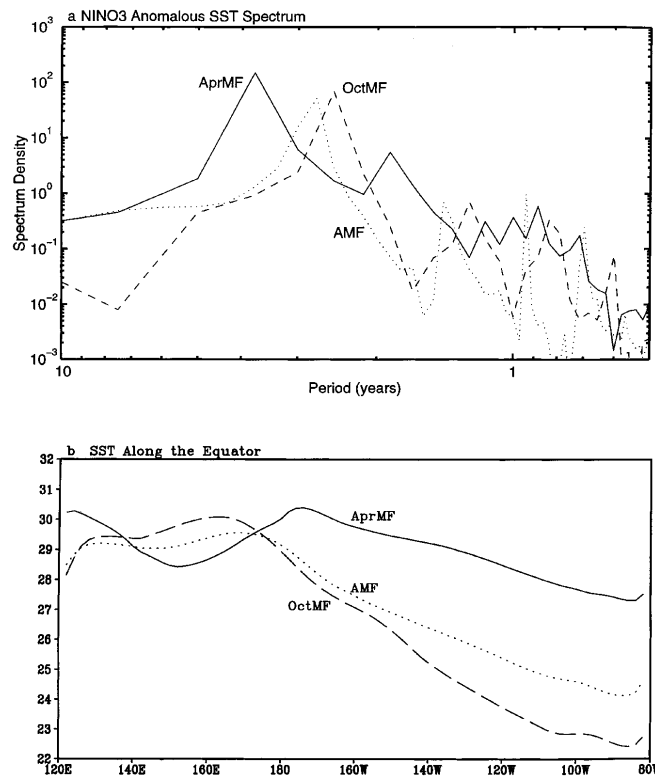

Fig. 12 a Spectra of Nino-3 SST anomalies and **b** long-term mean equatorial SST profiles simulated in the AMF (annual mean forcing) experiment (*solid*), OctMF (October mean forcing) experiment (*dashed*), and the AprMF (April mean forcing) experiments (*dotted*)

Fig. 13a, b Scattering diagram of Nino 3 SST anomalies as a function of calendar month **a** in the annual mean solar forcing experiment, and **b** in the control experiment. The *solid lines* in **a** and **b** show the mean positive and mean negative anomalies, respectively

6.2 Roles of the ITCZ and western Pacific monsoons

The annual cycle forcing may affect ENSO via changing convective heating and wind stress and associated thermocline displacement. The annual variations of thermocline depth are primarily controlled by the annual march of the eastern Pacific ITCZ and the western Pacific monsoon (Wang et al. submitted 1998). A natural
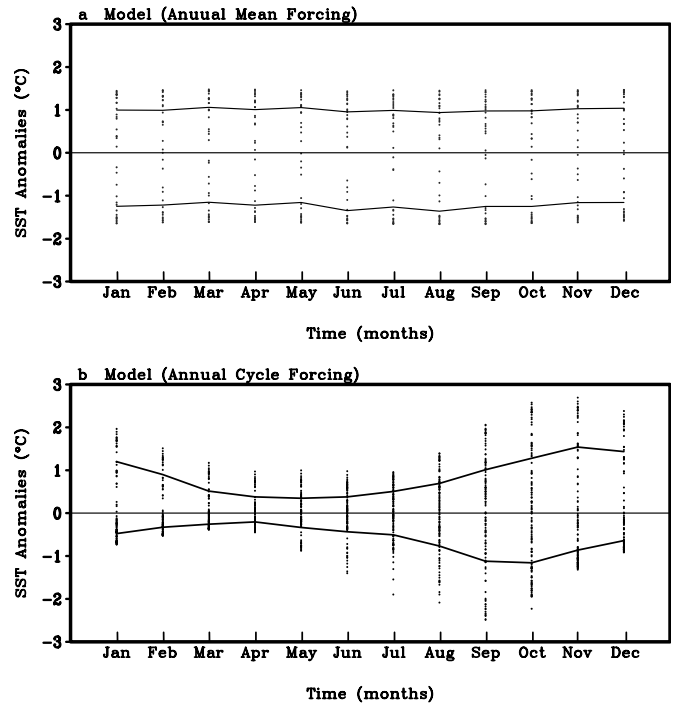
question to ask is how different are the influences of the annual cycle of the two wind systems on ENSO?

Two experiments are designed to isolate the impacts of the western Pacific monsoon and the eastern Pacific ITCZ. In these two experiments, the model parameters are identical with the control experiment except that in the eastern Pacific ITCZ experiment (EPAC) the forcing in the western Pacific (120°E–180°E) takes annual mean values, while in the western Pacific monsoon experiment (WPAC), the forcing in the eastern Pacific (160°W–80°W) takes annual mean values. In both experiments, the region between the dateline and 160°W is a buffer zone in which smoothed transition is designed to provide continuity in the external forcing. The purpose of the EPAC and WPAC experiments is to reveal the roles of the annual cycles associated with the eastern Pacific ITCZ and the western Pacific monsoon, respectively.

The long-term mean fields are similar in the two experiments as seen from the equatorial zonal wind profile (figure not shown). However, the annual cycles of the equatorial zonal wind differ. Compared to the control experiment, the annual cycle changes drastically in the longitudes where the annual mean forcing is used, while the annual cycle has little change in the longitudes where the annual cycle forcing is kept.

In response to the changes in the annual cycle forcing, the model's intrinsic oscillation changes characters primarily in their temporal structures but not in their spatial structure and propagation. The ENSO in
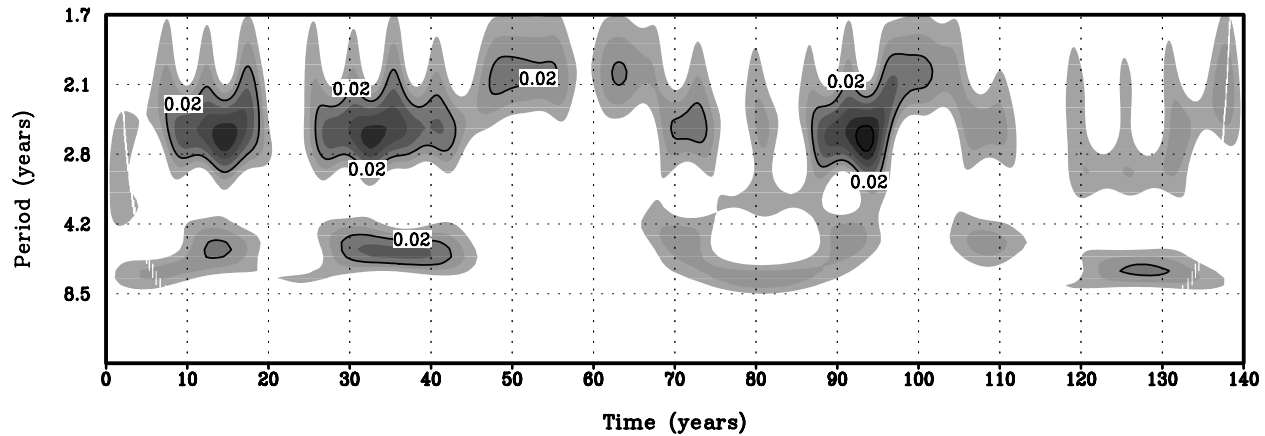
Fig. 14 Wavelet analysis of the Nino 3 SST anomalies simulated in the control experiment: modules as a function of period (year) and model integration year. The contour interval is 0.02 °C^2
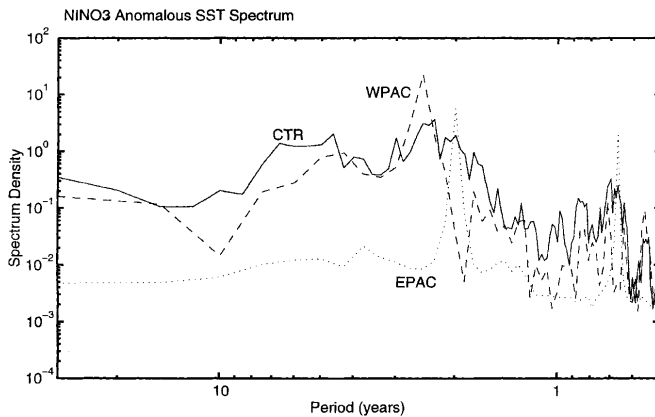

Fig. 15 The spectrum of the Nino-3 SST anomalies simulated in the control (*solid*), WPAC (*dashed*), and EPAC (*dotted*) experiments

EPAC experiment shows regular biennial oscillation with substantially reduced amplitude, whereas the ENSO in the WPAC experiment shows irregular oscillation with an amplitude comparable to the control run and a dominant period of 2.6 years and a secondary periodicity occurring in the 4–5 year time scale (Fig. 15). In general, the oscillation in WPAC experiments is similar to the oscillation in the control experiment, but the energy tends to concentrate more in the 2–3 year oscillation.

Comparison of the results derived from these two experiments with those of the control experiment indicates that the western Pacific monsoon generates irregularities and the bi-time scales (the biennial and low-frequency component); without the western Pacific monsoon, the model ENSO is much weaker and regular. The annual variation of the eastern Pacific ITCZ, on the other hand, favors the model ENSO phase locking to the annual cycle and favor the biennial oscillation. The low-frequency oscillation component is strongest when both the annual cycle forcing in the western and eastern Pacific exists.

7 Discussion

The coupled tropical ocean-atmospheric model presented represents a new class of the coupled models, which are distinctive from the anomaly models such as Zebiak and Cane (1987) and the complex CGCMs. The model is capable of realistic simulation of both the climatology and interannual fluctuations of key variables of the coupled climate system without explicit flux correction or anomaly coupling. The simulated interannual variations resemble ENSO in the following aspects: the coherent spatial structure between the equatorial SST, the surface zonal winds and rainfall anomalies; the multi-time scales of the interannual variability, in particular, the quasi-biennial and the low-frequency components of the oscillation; the chaotic irregularity; the interdecadal modulation of amplitude and periodicity; and the phase-locking of ENSO to the annual cycle. The simulated climatological mean state and annual cycle are also realistic, in particular, the equatorial east-west temperature gradient and associated zonal winds which are most critical to simulation of ENSO, the predominant annual evolution of the equatorial cold tongue and associated annual march of the ITCZ, and the latitudinal climate asymmetry in the eastern Pacific.

The interdecadal modulation of the amplitude and frequency of the model ENSO suggests that the interdecadal variability of ENSO cycles may be generated internally within the tropics and without the influence of the extratropics. This does not mean that the interaction between the tropics and extratropics is not important for the interdecadal variations of ENSO. However, it does suggest an alternative possible mechanism, which is operating in the coupled tropical ocean-atmosphere system. This mechanism relies on the existence of the multi-time scale components of ENSO. The quasi-biennial and low-frequency components of model ENSO interact with the climatological mean state. The nonlinear interaction rectifies the mean climate, which in turn regulates the relative strength of the two compo-

nents, generating the variability in amplitude and dominant frequency. This mechanism deserves further investigation.

One of the major deficiencies of the present ICOAM lies in the lack of atmospheric transients. These high frequency fluctuations involve dynamics different from that of ENSO and may act as stochastic forcing to the slowly evolving coupled ocean-atmospheric system. They can play important roles in model's interannual oscillation. The irregular oscillation obtained in the present model is of low-order chaos and relies on coupled instability. However, the numerical model study of Flugel and Chang (1996) and theoretical model study of Wang et al. (1999) indicate that, in a stable regime of the coupled dynamic system in which the coupled dynamics cannot sustain intrinsic oscillation, stochastic forcing may excite low-frequency oscillation that is otherwise damped. Because of the lack of high-frequency fluctuations, the model generated ENSO-like oscillation is much more regular compared with observed ENSO.

Another weakness of the model is related to the specification of the cloudiness in computation of the atmospheric radiation cooling and downward heat flux to the ocean mixed layer. While this specification benefits simulation of the coupled mean climate, it does not allow study of the cloud-radiation-SST feedback process. A scheme in which cloud is interactive with atmospheric circulations is currently under development.

The model ENSO-like oscillation captures some essential features of the observed ENSO, such as multi-time scales (the quasi-biennial and low frequency components) and the phase locking to annual cycles. A full understanding the causes that are responsible for these characteristics may improve our understanding the behavior of the observed ENSO or ENSO-like oscillations simulated in complex CGCMs. This remains a challenge. The results from our current endeavor will be reported later.

References

Anderson DLT, McCreary JP (1985) Slowly propagating disturbances in a coupled ocean-atmosphere model. J Atmos Sci 42: 615–629

Arakawa A, Katayama A, Mintz Y (1969) Numerical simulation of the general circulation of the atmosphere. In: Proc WMO/IUGG Symp Numerical Weather Prediction in Tokyo, Meteorology Society Japan Tokyo, pp IV.7–IV.8

Barnett TP, Graham N, Latif M (1991) Origins of the quasi-biennial oscillation in Tropical Pacific. Proc 16th Climate Diagnostic Workshop 16: 1–4

Bjerknes J (1969) Atmospheric teleconnections from the equatorial Pacific. Mon Weather Rev 97: 163–172

Cane MA, Moore DW (1981) A note on low-frequency equatorial basin modes. J Phys Oceanogr 11: 1578–1584

Cane MA, Zebiak SE, Dolan SC (1986) Experimental forecasts of El Nino. Nature 321: 827–832

Chang P, Wang B, Li T, Ji L (1994) Interactions between the seasonal cycle and the Southern Oscillation – frequency entrainment and chaos in an intermediate coupled ocean- atmosphere model. Geophys Res Lett 21: 2817–2820

Chang P, Ji L, Flugel M (1996) Chaotic dynamics versus stochastic processes in El Nino-Southern Oscillation in coupled-atmosphere models. Physica D 98: 301–320

Flugel M, Chang P (1996) Impact of dynamical and stochastic processes on the predictability of ENSO. Geophys Res Lett 23: 2089–2092

Fu X, Wang B (1998) On the role of longwave radiation and boundary layer thermodynamics in forcing tropical surface winds. J Clim (in press)

Gu D, Philander SGH (1995) Secular changes of annual and interannual variability in the tropics during the past century. J Clim 8: 864–876

Gill AE (1980) Some simple solutions for heat-induced tropical circulation. Q J R Meteorol Soc 106: 447–462

Hirst AC (1986) Unstable and damped equatorial modes in simple coupled ocean-atmosphere models. J Atmos Sci 43: 606–630

Ji M, Leetmaa A, Kousky V (1996) Coupled model predictions of ENSO during the 1980s and 1990s at the National Center for Environmental Prediction. J Clim 9: 3155–3120

Kleeman R (1993) On the dependence of hindcast skill in a coupled ocean-atmosphere model on ocean thermodynamics. J Atmos Sci 48: 3–18

Latif M, Sterl A, Maier-Reimer E, Junge MM (1993) Climate variability in a coupled GCM. Part I: the tropical Pacific. J Clim 6: 5–21

Lau N-C, Philander SGH, Nath MJ (1992) Simulation of ENSO-like phenomena with a low-resolution coupled GCM of the global ocean and atmosphere. J Clim 5: 284–307

Li T, Wang B (1994) A thermodynamic equilibrium climate model for monthly mean surface winds and precipitation over the tropical Pacific. J Atmos Sci 51: 1372–1385

Lindzen RS, Nigam S (1987) On the role of sea surface temperature gradients in forcing low-level winds and convergence in the tropics. J Atmos Sci 45: 2440–2458

Mechoso CR, Coauthors (1995) The seasonal cycle over tropical Pacific in coupled ocean-atmosphere models. Mon Weather Rev 123: 2835–2838

Matsuno T (1966) Numerical integration of primitive equation by use of a simulated backward difference method. J Meteorol Soc Japan, Ser II 44: 76–84

Matthews E (1983) Global vegetation of land use: new high-resolution databases for climate studies. J Clim Appl Meteorol 22: 474–487

Miller MJ, Thorpe AJ (1981) Radiational conditions for the lateral boundaries of limited area numerical models. Q J R Meteorol Soc 107: 615–628

Neelin JD (1991) The slow sea surface temperature mode and the fast-wave limit: analytic theory for tropical interannual oscillations and experiments in a hybrid coupled model. J Atmos Sci 48: 584–606

Neelin JD, Coauthors (1992) Tropical air-sea interaction in general circulation models. Clim Dyn 7: 73–104

Niller PP, Kraus EB (1977) One-dimensional models of upper ocean. In: Kraus EB (ed) Modeling and prediction of the upper layers of the ocean. Pergamon Press, Oxford, pp 143–172

Oberhuber JM (1988) An atlas based on the "COADS" data set: the budget of heat, buoyancy and turbulent kinetic energy at the surface of the global ocean. Max-Planck Institut fuer Meteorologie, Rep 15, 196 pp

Philander SGH, Yamagata T, Pacanowski RC (1984) Unstable air-sea interactions in the tropics. J Atmos Sci 41: 604–613

Philander SGH, Pacanowski RC, Lau NC, Nath MJ (1992) Simulation of ENSO with a global atmospheric GCM coupled to a high-resolution, tropical Pacific ocean GCM. J Clim 5: 308–329

Rasmusson EM, Wang X, Ropelewski CF (1990) The biennial component of ENSO variability. J Mar Syst 1: 79–96

Ropelewski CF, Halpert MS (1992) Observed tropospheric biennial variability and its relationship to the Southern Oscillation. J Clim 5: 594–614

Sadler JC, Lander MA, Hori AM, Oda LK (1987) Tropical marine climate atlas. Report UHMET 87-02, Department of Meteorology, University of Hawaii, Honolulu, Hawaii

Schopf PS, Suarez MJ (1988) Vacillation in a coupled ocean-atmosphere model. J Atmos Sci 45: 549–566

Seager RM, Blumenthal B, Kushnir Y (1995) An advective atmospheric mixed layer model for ocean modeling purposes: global simulation of surface heat fluxes. J Clim 8: 1951–1964

Shapiro R (1970) Smoothing, filtering, and boundary effects. Rev Geophys Space Phys 8: 359–387

Shuman FG (1957) Numerical methods in weather predication. II. Smoothing and filtering. Mon Weather Rev 85: 3579–3587

Suarez MJ, Schopf PS (1988) A delayed action oscillator for ENSO. J Atmos Sci 45: 3283–3287

Wakata Y, Sarachik ES (1991) Unstable coupled atmosphere-ocean basin modes in the presence of a spatially varying basic state. J Atmos Sci 48: 2060–2070

Wang B (1988) The dynamics of tropical low frequency waves: an analysis of moist Kelvin waves. J Atmos Sci 45: 2051–2065

Wang B (1994) On the annual cycle in the tropical eastern central Pacific. J Clim 7: 1926–1942

Wang B, Li T (1993) A simple tropical model of relevance to short-term climate variations. J Atmos Sci 50: 260–284

Wang B, Wang Y (1996) Temporal structure of the southern oscillation as revealed by waveform and wavelet analysis. J Clim 9: 1586–1598

Wang B, Fang Z (1996) Chaotic oscillation of tropical climate: a dynamic system theory for ENSO. J Atmos Sci 53: 2786–2802

Wang B, Li T, Chang P (1995) An intermediate model of the tropical Pacific Ocean. J Phys Oceanogr 25: 1599–1616

Wang B, Wu R, Lukas R (1998) Roles of the western North Pacific wind variation in thermocline adjustment and ENSO phase transition. J Meteorol Soc Japan, (in press)

Wang B, Barcilon A, Fang Z (1999) Stochastic dynamics of El Nino-Southern Oscillation. J Atmos Sci 56: 5–23

Wu J (1969) Wind stress and surface roughness at air-sea interface. J Geophys Res 74: 444–455

Xie PP, Arkin PA (1996) Analyses of global monthly precipitation using gauge observations, satellite estimates, and numerical model predictions. J Clim 9: 840–858

Zebiak SE, Cane MA (1987) A model El Nino – Southern Oscillation. Mon Weather Rev 115: 2262–2278